THE JOURNAL OF PHYSICAL CHEMISTRY Letters

Letter

pubs.acs.org/JPCL

Octahedral Rotation Preferences in Perovskite Iodides and Bromides

Joshua Young*,† and James M. Rondinelli*,‡

†Department of Materials Science and Engineering, Drexel University, Philadelphia, Pennsylvania 19104, United States

‡Department of Materials Science and Engineering, Northwestern University, Evanston, Illinois 60208, United States

Supporting Information

ABSTRACT: Phase transitions in ABX_3 perovskites are often accompanied by rigid rotations of the corner-connected BX_6 octahedral network. Although the mechanisms for the preferred rotation patterns of perovskite oxides are fairly well recognized, the same cannot be said of halide variants (i.e., X = Cl, Br, or I), several of which undergo an unusual displacive transition to a tetragonal phase exhibiting in-phase rotations about one axis ($a^0a^0c^+$ in Glazer notation). To discern the chemical factors stabilizing this unique phase, we investigated a series of 12 perovskite bromides and iodides using density functional theory calculations and compared them with similar oxides. We find that in-phase tilting provides a better arrangement of the larger bromide and iodide anions, which minimizes the electrostatic interactions, improves the bond valence of the A-site cations, and enhances the covalency between the A-site metal and Br^- or I^- ions. The opposite effect is present in the oxides, with out-of-phase tilting maximizing these factors.

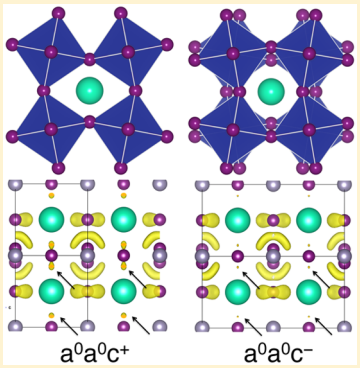

Perovskite materials of the form ABX_3 are becoming increasingly popular for technological applications, especially because of their highly flexible corner-connected BX_6 octahedral network and significant tunability resulting from their large degree of chemical variability.[1,2] Although perovskite oxides (X = O) are by far the most common variant of this family, the bromides (X = Br) and iodides (X = I) have garnered particular attention over the past few years for potential use in solar cells owing to their visible-region band gaps, low effective masses, and ease of production.[3,4] The main focus of this rapidly burgeoning field is on organic−inorganic hybrid perovskite halides (typically with A = CH_3NH_3); solar cells containing hybrid bromides have attained 10% conversion efficiency,[5] while those based on iodides have successfully reached up to 19%.[6] Furthermore, perovskite halides without organic constituents, such as $CsSnI_3$, have also successfully been integrated into solar devices (albeit with lower efficiencies).[7,8]

While these purely inorganic compounds exhibit desirable properties, they also undergo a unique series of phase transitions owing to different cooperative distortions to the BX_6 octahedral network. The degree to which the octahedral network rotates is well known to affect the magnetic, electronic, and optical properties of oxides;[2] although fewer systematic investigations have been performed for the perovskite halides, some studies have shown that, similar to oxides, the magnitude of the tilting has a strong effect on the band gap.[9,10] Consider the aforementioned $CsSnI_3$ as an example, which has four distinct polymorphs.[11,12] At high temperature, it is cubic with the prototypical undistorted $Pm\bar{3}m$ perovskite structure (i.e., $a^0a^0a^0$ in Glazer notation,[13] Figure 1a). Upon cooling, the material transitions to a tetragonal $P4/mbm$ phase with the appearance of in-phase rotations of the SnI_6 octahedral network about the c axis (an $a^0a^0c^+$ tilt pattern, Figure 1b); this occurs in

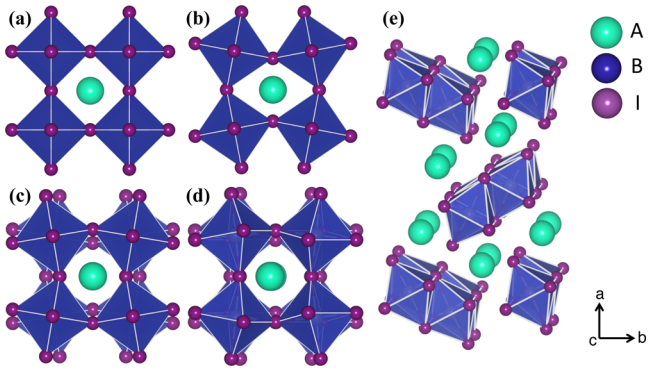

Figure 1. Phases of ABI_3 iodide perovskites considered are (a) cubic $a^0a^0a^0$ (space group $Pm\bar{3}m$, no. 221), (b) tetragonal $a^0a^0c^+$ ($P4/mbm$, no. 127), (c) tetragonal $a^0a^0c^-$ ($I4/mcm$, no. 140), (d) orthorhombic $a^-a^-c^+$ ($Pnma$, no. 62), and (e) orthorhombic face sharing ($Pnma$, no. 62).

several other halides, such as $RbSnBr_3$,[14] $CsSnBr_3$,[15,16] and $CsPbBr_3$.[17] Although a cubic-to-tetragonal phase transition is not uncommon in perovskite oxides, the presence of a phase containing only an in-phase rotation is highly unusual. Instead, oxides more commonly exhibit the $a^0a^0c^-$ $I4/mcm$ phase (such as in $CaTiO_3$ or $SrTiO_3$, Figure 1c). To the best of our knowledge, no simple oxides form in the $P4/mbm$ phase under ambient conditions;[18] we note, however, that $NaNbO_3$, $NaTaO_3$, and $AgNbO_3$ all undergo a complex series of six to seven phase transitions and do display a $P4/mbm$ structure at

Received: January 14, 2016
Accepted: February 20, 2016

© XXXX American Chemical Society

DOI: 10.1021/acs.jpclett.6b00094
J. Phys. Chem. Lett. 2016, 7, 918−922

high temperature (>660 K).[19−21] Upon further cooling, $CsSnI_3$ then transitions to the common orthorhombic *Pnma* phase with an $a^-a^-c^+$ tilt pattern Figure 1d), which is metastable to a nonperovskite structure exhibiting face-sharing 1D chains of SnI_6 octahedra (Figure 1e).

In this work, we seek to understand which chemical factors are responsible for these phase transitions and to elucidate the driving force for the stabilization of the in-phase tilt over the oxide-preferred out-of-phase tilt in the tetragonal bromide and iodide perovskites. Using first-principles density functional theory (DFT) methods,[22,23] we investigate six $ABBr_3$, six ABI_3, and two ABO_3 perovskites. We find that the in-phase rotation pattern, when compared to the out-of-phase pattern, provides greater electrostatic energy stabilization while also allowing the anions to better coordinate the *A*-site cations in the halide perovskites. These two trends are reversed in the oxides. The orthorhombic structure with the $a^-a^-c^+$ rotations further enhances the electrostatic stability and *A*-site bond preference compared to that achieved by either of the single tetragonal tilt systems for both the halides and oxides. Finally, we find that in some of the halides the 1D chain configuration provides the best configuration to minimize electrostatic repulsion, even though it somewhat overcoordinates the *A*-site compared to the perovskite phase. Investigating these structural preferences in halide perovskites can lead to a better understanding of the degradation of perovskite solar cells, or even novel types of geometric hybrid improper ferroelectrics based on cation ordering.[24−26]

Our DFT calculations were performed using projector-augmented wave (PAW) potentials[27] within the PBEsol functional,[28] as implemented in the Vienna ab initio Simulation Package (VASP).[29−31] A more detailed description of the computational methods and parameters is given in the Supporting Information (SI). The $ABBr_3$ and ABI_3 compounds were generated by substituting alkali metals on the *A*-site (*A* = Rb, Cs) and group IV elements on the *B*-site (*B* = Ge, Sn, Pb), resulting in 12 compounds: $RbGeBr_3$, $RbSnBr_3$, $RbPbBr_3$, $CsGeBr_3$, $CsSnBr_3$, $CsPbBr_3$, $RbGeI_3$, $RbSnI_3$, $RbPbI_3$, $CsGeI_3$, $CsSnI_3$, and $CsPbI_3$. In the Figures, we abbreviate each by using the first letters of the *A*- and *B*-site cations: C and R for Cs and Rb and G, S, and P for Ge, Sn, and Pb, respectively. We chose to study these specific compounds because each is experimentally known to exist in at least one of the five phases shown in Figure 1,[11,12,14−17,32−36] although not all of these compounds exhibit the same aforementioned phase-transition sequence exhibited by $CsSnI_3$. This series also allows for a systematic study on the effect of chemical substitution on the energetics of these rotations, which is necessary for disentangling the underlying physical origin; however, because our focus is on the general driving force for the stabilization of structures with in-phase tilts in halide perovskites rather than the particular effect of a specific chemistry on the structure, we enforce and investigate each of the tilt patterns in Figure 1 for all chemistries and use the results to draw general conclusions across the family. Finally, although the chloride analogues to some of these compounds exist in many of the phases, the entire series (A = Cs, Rb and B = Sn, Pb) has yet to fully synthesized.

The two oxides we chose for comparison are $CaTiO_3$ and $SrTiO_3$. $CaTiO_3$, similar to $CsSnI_3$, undergoes a cubic-to-tetragonal-to-orthorhombic phase transition; the tetragonal phase here, however, exhibits an *I*4/*mcm* space group and $a^0a^0c^-$ tilt pattern.[37] $SrTiO_3$ is nominally cubic $Pm\bar{3}m$ at room temperature but develops a very small out-of-phase tilt about the tetragonal axis under pressure[38] or below 110 K.[39]

We first fixed all 14 of the aforementioned compounds to the five phases shown in Figure 1 and performed relaxations of the lattice and atomic degrees of freedom. The equilibrium lattice constant of the iodide materials is always larger than the bromide analogues owing to the larger size of iodide ion; this is consistent with experimental results showing that increasing the bromide content in mixed $AB(Br_{3-x}I_x)$ halide systems systematically decreases the lattice parameter according to Vegard's law.[42] In four of the bromides and five of the iodides, we found that the cubic phase was higher in energy than the tetragonal phases, which, in turn, was higher than the orthorhombic perovskite phase (see SI, Figure S1); the 1D chain structure was the lowest energy phase for all compounds. We then found that when comparing the two tetragonal phases, the $a^0a^0c^+$ tilt pattern was always lower in energy than $a^0a^0c^-$ for each of the 12 halide compounds (Figure 2a,b, bottom panels); additionally, the in-phase tilt angle amplitude was always slightly larger than that of the out-of-phase tilt angle (Figure 2a,b, top panels). In the oxides, while the same general energetic ordering of the cubic, tetragonal, and orthorhombic phases is observed, the presence of the $a^0a^0c^-$ phase now lowers the energy more than the $a^0a^0c^+$ tilt (Figure 2c).

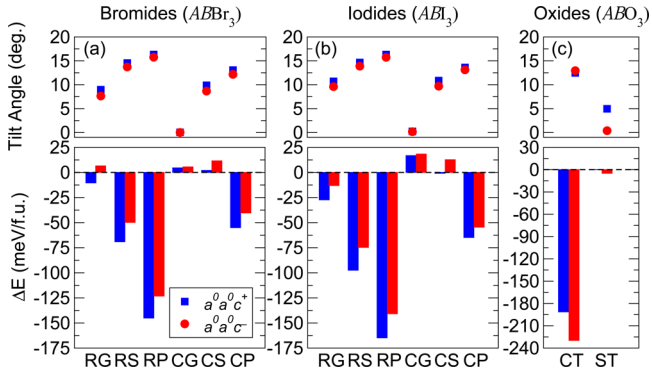

Figure 2. Comparison of the energy of the $a^0a^0c^+$ (blue) and $a^0a^0c^-$ (red) tilt patterns in each of the six bromides (left), six iodides (middle), and oxides (right). The energy is taken with respect to the cubic phase of each compound. In each of the halides, the phase containing the in-phase rotations is always lower in energy than that containing the out-of-phase tilt pattern; in the two oxides, the energy of the out-of-phase tilting is always lower (bottom panels). The magnitude of each tilt is similar in each compounds, with the size of the in-phase rotations being slightly larger than the out-of-phase tilts in the halides (top panels). The general trend here captures that found in experiment, with the in-phase tilt angle of the iodides being slightly larger than bromides (6.01° for $CsSnI_3$[12] and ∼2 to 3° for $CsSnBr_3$[16]) and the out-of-phase tilt angle of $CaTiO_3$ (7.63°)[37] being larger than $SrTiO_3$ (1.12°).[40] Note that our DFT calculations systematically overestimate the tilt angle as expected owing to the exchange-correlation functional.[41]

The general trend of octahedral rotations being favorable in perovskite oxides is fairly well understood.[43,44] The vast number of known perovskites undergo some form of octahedral rotations owing to a mismatch between the size of the *A*-site cation and the spaces between the BX_6 network,[18,45,46] as described by the Goldschmidt tolerance factor,[47] $\tau = (r_A + r_O)/\sqrt{2}(r_B + r_O)$, where r_A, r_B, and r_O are the ionic radii of the *A*-site, *B*-site, and oxide ions, respectively. A compound with a tolerance factor close to 1 is typically predicted to be cubic, as it

DOI: 10.1021/acs.jpclett.6b00094
J. Phys. Chem. Lett. 2016, 7, 918−922

indicates that the *A*-site cation is the appropriate size to fit in the interstices. Octahedral tilt patterns of some form are predicted for materials with $\tau < 1$ due to a too-small *A* cation; because of the undercoordination of the cation, the octahedra tilt in an attempt to enhance the covalency and improve the *A*–O interactions. This argument is indeed captured in the energy of the compounds we investigated here. (For a tabulation of the tolerance factors of these compounds, see SI, Table S1.) In those compounds with τ close to 1, such as $CsGeBr_3$ ($\tau = 1.01$), $CsSnBr_3$ ($\tau = 0.931$), and $CsGeI_3$ ($\tau = 0.997$), the enforcement of any tilt pattern results in an (unfavorable) increase in energy. In others, such as $RbGeBr_3$ ($\tau = 0.967$) and $CsSnI_3$ ($\tau = 0.901$), the out-of-phase tilt raises the energy while the in-phase tilt slightly lowers it. Finally, the tolerance factor for the remaining compounds ranges from 0.858 to 0.898, and any rotation pattern lowers the energy. Plotting the energy of each phase as a function of tolerance factor (SI, Figure S2) supports this trend.

Although these results are anticipated, they do not answer the question of why the *P*4/*mbm* tetragonal phase is preferred in the halides, while the *I*4/*mcm* phase is more stable in the oxides. To further investigate this, we computed the electrostatic contribution to the total energy (ΔE_{ES}) of each tilt pattern within each compound. These results are shown in Figure 3, with each energy being computed at the equilibrium

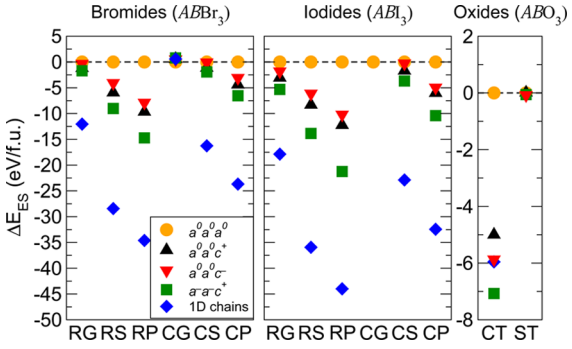

Figure 3. Electrostatic energy (ΔE_{ES}) of each compound taken with respect to the cubic phase (orange circles). In each of the bromides and iodides, the $a^0a^0c^+$ rotation pattern (black triangles) is lower in energy than the $a^0a^0c^-$ (red inverted triangle) one, indicating a more favorable arrangement of the ions. In the oxides, the opposite is observed. The $a^+b^-b^-$ pattern (green squares) is, in general, lower than either of these owing to the ability of the *A*-sites to off-center, with the 1D chain configuration (blue diamonds) then being the lowest among the considered halide polymorphs.

rotation angle and taken with reference to the cubic $Pm\bar{3}m$ phase. The first thing to note is that in each halide where the presence of octahedral rotations lowers the energy, the electrostatic energy of the tetragonal phase with in-phase tilting is always slightly more negative than the phase with the out-of-phase tilting, indicating a more favorable electrostatic arrangement of the atoms. Additionally, ΔE_{ES} of the orthorhombic $a^-a^-c^+$ tilt pattern is even lower than either tetragonal phase owing to the now symmetry-allowed *A*-site cation displacements; the 1D chain configuration is also the most favorable. In those compounds where tilting leads to an energetic penalty, such as $CsGeBr_3$ and $CsGeI_3$, ΔE_{ES} is positive with respect to the cubic phase (several of the energy values for these are too high to be reasonably displayed in the Figure), another confirmation of the aforementioned tolerance factor analysis.

The opposite trend is observed in $CaTiO_3$. Now ΔE_{ES} of the $a^0a^0c^-$ tilt pattern is slightly lower than the $a^0a^0c^+$. To ensure this result was not an artifact of the amplitude of the different in-phase and out-of-phase rotation amplitudes, we next computed ΔE_{ES} for $CsSnI_3$ and $CaTiO_3$ at a variety of rotation angles in which the in-phase and out-of-phase rotations were set to the same magnitude. Indeed, we find the same trend for both compounds as when their rotations are at equilibrium (SI, Figure S3). The $a^-a^-c^+$ rotations offer the best electrostatic coordination in the oxides, as the 1D chain configuration is no longer the lowest in energy. In $SrTiO_3$, all tilt patterns give approximately the same ΔE_{ES}, similar to $CsGeBr_3$.

We next computed the bond valence sum of the *A*-site cation in each phase. By comparing the bond valence of the *A*-site cation to its nominal valence (+1 for Rb and Cs in the halides, + 2 for Ca and Sr in the oxides), we are able to assess how well the anion configurations derived from the different tilt patterns coordinate it (Figure 4, bottom panels). In all six of the

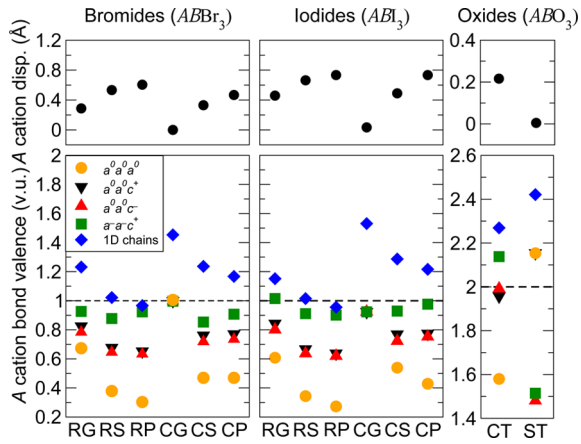

Figure 4. Bond valence sums of the *A*-site cations in each of the bromide, iodide, and oxide compounds in each of the five atomic configurations (bottom). The cubic tilt pattern coordinates the cations the worst. In the two tetragonal phases, the $a^0a^0c^+$ tilt pattern better coordinates the *A*-sites than the $a^0a^0c^-$ tilt pattern in the halides, with the trend reversed in the oxides. The $a^-a^-c^+$ provides the best coordination, owing to the *A*-site displacements, the magnitude of which are shown in the top panels. The 1D chain configuration tends to overcoordinate the cations.

bromides and five of the six iodides, the trend of the *A*-site bond valence is relatively the same in that the untilted cubic phase highly under-coordinates the Rb or Cs atoms. Furthermore, although the two tetragonal tilt patterns ($a^0a^0c^-$ and $a^0a^0c^+$) provide approximately the same coordination, the bond valence of the *A*-site in compounds exhibiting an in-phase tilt is always slightly higher (closer to 1) than that with an out-of-phase, indicating a better coordination environment. In $CaTiO_3$, this trend is reversed, with the out-of-phase rotations putting the bond valence of the Ca atom closer to the preferred +2 state than the in-phase rotations.

The orthorhombic $a^-a^-c^+$ phase provides the best coordination, keeping the *A*-site atoms close to their preferred +1 or +2 oxidation state. This is due to the fact that in the *Pnma* space group the *A*-site cations are allowed to displace; the displacement magnitudes are shown in the upper panels of Figure 4. In both the halides and oxides, the 1D chain configuration has a tendency to overcoordinate the *A*-site; the preference for certain halides to adopt this phase is thus a

DOI: 10.1021/acs.jpclett.6b00094
J. Phys. Chem. Lett. 2016, 7, 918–922

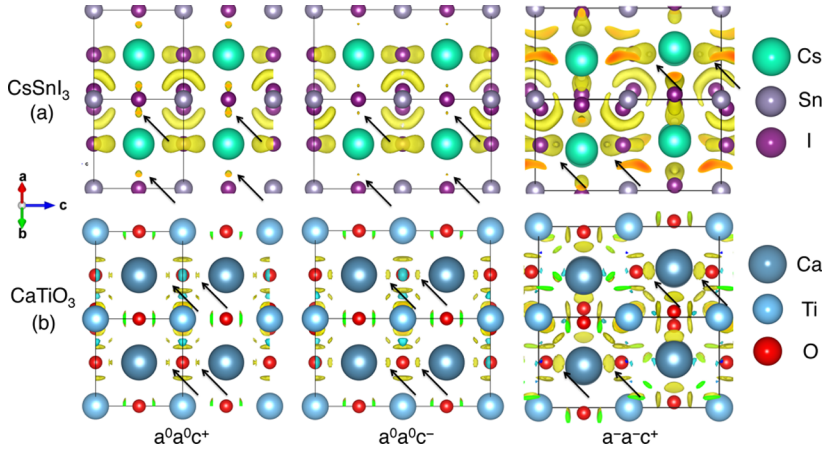

Figure 5. Charge density of (a) $CsSnI_3$ and (b) $CaTiO_3$ when fixed to an $a^0a^0c^+$ (left), $a^0a^0c^-$ (center), or $a^-a^-c^+$ (right) tilt pattern. There is a greater excess of charge between the *A*-site and iodide ions when the in-phase tilt is present in the halide, while the same is true of the out-of-phase tilt in the oxide. The mixed tilt $a^-a^-c^+$ phase shows a greater excess than either of the two tetragonal phases, along with a local asymmetry to the charge density owing to *A*-site displacements.

balance between the better electrostatic arrangement it offers and the resulting overcoordination. Interestingly, the greater the allowed *A*-site displacements in the $a^-a^-c^+$ phase, the *better* the coordination supplied by the 1D chain structure. Within the oxides, the fact that this arrangement does not offer any electrostatic benefit in addition to overcoordinating the *A*-site may provide a suitable crystal chemistry explanation as to why this phase is not experimentally observed.

These results are further reflected in the charge density of the compounds, which we computed for $CsSnI_3$ and $CaTiO_3$. To make a more meaningful comparison, we froze the magnitude of the out-of-phase rotation in $a^0a^0c^-$ to that of the equilibrium in-phase $a^0a^0c^+$ structure. We find that in $CsSnI_3$ (Figure 5a) there is a much larger overlap between the Cs and I atoms in the tetragonal phase with the in-phase tilt rather than the out-of-phase tilt. This enhanced covalent character seems, in part, to be important to the stability of this tilt pattern, as further reflected by the bond valence parameters shown in Figure 4. The $a^-a^-c^+$ tilt pattern has a greater excess of charge located along the "bond" with the anions than either of the two tetragonal phases, further suggesting the importance of *A*-*X* covalency in tilt pattern stabilization. The effect of the symmetry-allowed *A*-site displacements in the *Pnma* phase is also reflected in the now locally asymmetric charge density. The opposite charge density changes are observed in the oxides. In $CaTiO_3$ (Figure 5b), the out-of-phase tilt exhibits more excess charge density between the Ca and O atoms compared with the in-phase tilt. The orthorhombic $a^-a^-c^+$ phase, however, displays similar features to that of the iodide.

In conclusion, we investigated the presence of the unusual *P*4/*mbm* tetragonal phase displaying only in-phase BX_6 octahedral rotations ($a^0a^0c^+$) in the bromide and iodide perovskite families. Our results show that in the presence of these large halide ions the electrostatic interactions are optimized by this tilt pattern rather than the more common $a^0a^0c^-$ rotations found in the oxide analogues. Furthermore, the $a^0a^0c^+$ tilt better coordinates the *A*-site atoms, as shown by computation of bond valence sums. Finally, these in-phase rotations result in enhanced covalency between the *A*-site and halide ions, in contrast with the oxides in which the out-of-phase rotations are stabilized. These aspects together give useful chemical insight for the stabilization of this unique tilt pattern and will hopefully provide a foundation for the further study of the less-explored family of inorganic perovskite halides.

■ ASSOCIATED CONTENT

Ⓢ Supporting Information

The Supporting Information is available free of charge on the ACS Publications website at DOI: 10.1021/acs.jpclett.6b00094.

Computational parameters and additional data for all compounds. (PDF)

■ AUTHOR INFORMATION

Corresponding Authors

*J.Y.: E-mail: jy346@drexel.edu.

*J.M.R.: E-mail: jrondinelli@northwestern.edu.

Notes

The authors declare no competing financial interest.

■ ACKNOWLEDGMENTS

J.Y. and J.M.R. were supported by the National Science Foundation under grant nos. DMR-1454688 and DMR-1420620, respectively. DFT calculations were performed on hardware supported by Drexel's University Research Computing Facility as well as the CARBON cluster at the Center for Nanoscale Materials (Argonne National Laboratory, also supported by DOE-BES DE-AC02-06CH11357).

■ REFERENCES

(1) Zhu, J.; Li, H.; Zhong, L.; Xiao, P.; Xu, X.; Yang, X.; Zhao, Z.; Li, J. Perovskite Oxides: Preparation, Characterizations, and Applications in Heterogeneous Catalysis. *ACS Catal.* **2014**, *4*, 2917−2940.

(2) Rondinelli, J. M.; May, S. J.; Freeland, J. W. Control of Octahedral Connectivity in Perovskite Oxide Heterostructures: An Emerging Route to Multifunctional Materials Discovery. *MRS Bull.* **2012**, *37*, 261−270.

(3) Snaith, H. J. Perovskites: The Emergence of a New Era for Low-Cost, High-Efficiency Solar Cells. *J. Phys. Chem. Lett.* **2013**, *4*, 3623−3630.

(4) Yin, W.-J.; Yang, J.-H.; Kang, J.; Yan, Y.; Wei, S.-H. Halide Perovskite Materials for Solar Cells: A Theoretical Review. *J. Mater. Chem. A* **2015**, *3*, 8926−8942.

(5) Heo, J. H.; Song, D. H.; Im, S. H. Planar $CH_3NH_3PbBr_3$ Hybrid Solar Cells with 10.4% Power Conversion Efficiency, Fabricated by

DOI: 10.1021/acs.jpclett.6b00094
J. Phys. Chem. Lett. 2016, 7, 918−922

Controlled Crystallization in the Spin-Coating Process. *Adv. Mater.* **2014**, *26*, 8179−8183.
(6) Zhou, H.; Chen, Q.; Li, G.; Luo, S.; Song, H.-S.; Duan, T.-b.; Hong, Z.; You, J.; Liu, Y.; Yang, Y. Interface Engineering of Highly Efficient Perovskite Solar Cells. *Science* **2014**, *345*, 542−546.
(7) Kumar, M. H.; Dharani, S.; Leong, W. L.; Boix, P. P.; Prabhakar, R. R.; Baikie, T.; Shi, C.; Ding, H.; Ramesh, R.; Asta, M.; et al. Lead-Free Halide Perovskite Solar Cells with High Photocurrents Realized Through Vacancy Modulation. *Adv. Mater.* **2014**, *26*, 7122−7127.
(8) Marshall, K. P.; Walton, R. I.; Hatton, R. A. Tin Perovskite/Fullerene Planar Layer Photovoltaics: Improving the Efficiency and Stability of Lead-Free Devices. *J. Mater. Chem. A* **2015**, *3*, 11631−11640.
(9) Filip, M. R.; Eperon, G. E.; Snaith, H. J.; Giustino, F. Steric Engineering of Metal-Halide Perovskites with Tunable Optical Band Gaps. *Nat. Commun.* **2014**, *5*, 5757.
(10) Grote, C.; Berger, R. F. Strain Tuning of Tin Halide and Lead Halide Perovskites: A First-Principles Atomic and Electronic Structure Study. *J. Phys. Chem. C* **2015**, *119*, 22832−22837.
(11) Yamada, K.; Funabiki, S.; Horimoto, H.; Matsui, T.; Okuda, T.; Ichiba, S. Structural Phase Transitions of the Polymorphs of $CsSnI_3$ by Means of Rietveld Analysis of the X-Ray Diffraction. *Chem. Lett.* **1991**, *20*, 801−804.
(12) Chung, I.; Song, J.-H.; Im, J.; Androulakis, J.; Malliakas, C. D.; Li, H.; Freeman, A. J.; Kenney, J. T.; Kanatzidis, M. G. $CsSnI_3$: Semiconductor or Metal? High Electrical Conductivity and Strong Near-Infrared Photoluminescence from a Single Material. High Hole Mobility and Phase-Transitions. *J. Am. Chem. Soc.* **2012**, *134*, 8579−8587.
(13) Glazer, A. M. The Classification of Tilted Octahedra in Perovskites. *Acta Crystallogr., Sect. B: Struct. Crystallogr. Cryst. Chem.* **1972**, *28*, 3384−3392.
(14) Kuok, M. H.; Tan, L. S.; Shen, Z. X.; Huan, C. H.; Mok, K. F. Structural Phase Transitions in $RbSnBr_3$. *Solid State Commun.* **1996**, *97*, 497−501.
(15) Scaife, D. E.; Weller, P. F.; Fisher, W. G. Crystal Preparation and Properties of Cesium Tin(II) Trihalides. *J. Solid State Chem.* **1974**, *9*, 308−314.
(16) Mori, M.; Saito, H. An X-Ray Study of Successive Phase Transitions in $CsSnBr_3$. *J. Phys. C: Solid State Phys.* **1986**, *19*, 2391−2401.
(17) Hirotsu, S.; Harada, J.; Iizumi, M.; Gesi, K. Structural Phase Transitions in $CsPbBr_3$. *J. Phys. Soc. Jpn.* **1974**, *37*, 1393−1398.
(18) Lufaso, M. W.; Woodward, P. M. Prediction of the Crystal Structures of Perovskites using the Software Program. *Acta Crystallogr., Sect. B: Struct. Sci.* **2001**, *57*, 725−738.
(19) Megaw, H. D. The Seven Phases of Sodium Niobate. *Ferroelectrics* **1974**, *7*, 87−89.
(20) Darlington, C. N. W.; Knight, K. S. High-Temperature Phases of $NaNbO_3$ and $NaTaO_3$. *Acta Crystallogr., Sect. B: Struct. Sci.* **1999**, *55*, 24−30.
(21) Sciau, P.; Kania, A.; Dkhil, B.; Suard, E.; Ratuszna, A. Structural Investigation of $AgNbO_3$ Phases Using X-Ray and Neutron Diffraction. *J. Phys.: Condens. Matter* **2004**, *16*, 2795−2810.
(22) Hohenberg, P.; Kohn, W. Inhomogeneous Electron Gas. *Phys. Rev.* **1964**, *136*, B864−B871.
(23) Kohn, W.; Sham, L. J. Self-Consistent Equations Including Exchange and Correlation Effects. *Phys. Rev.* **1965**, *140*, A1133.
(24) Benedek, N. A.; Fennie, C. J. Hybrid Improper Ferroelectricity: A Mechanism for Controllable Polarization-Magnetization Coupling. *Phys. Rev. Lett.* **2011**, *106*, 107204.
(25) Rondinelli, J. M.; Fennie, C. J. Octahedral Rotation-Induced Ferroelectricity in Cation Ordered Perovskites. *Adv. Mater.* **2012**, *24*, 1961.
(26) Young, J.; Stroppa, A.; Picozzi, S.; Rondinelli, J. M. Anharmonic Lattice Interactions in Improper Ferroelectrics for Multiferroic Design. *J. Phys.: Condens. Matter* **2015**, *27*, 283202.
(27) Blöchl, P. E. Projector Augmented-Wave Method. *Phys. Rev. B: Condens. Matter Mater. Phys.* **1994**, *50*, 17953−17979.
(28) Perdew, J. P.; Ruzsinszky, A.; Csonka, G. I.; Vydrov, O. A.; Scuseria, G. E.; Constantin, L. A.; Zhou, X.; Burke, K. Restoring the Density-Gradient Expansion for Exchange in Solids and Surfaces. *Phys. Rev. Lett.* **2008**, *100*, 136406.
(29) Kresse, G.; Hafner, J. *Ab initio* Molecular Dynamics for Liquid Metals. *Phys. Rev. B: Condens. Matter Mater. Phys.* **1993**, *47*, 558−561.
(30) Kresse, G.; Furthmüller, J. Efficiency of ab-initio Total Energy Calculations for Metals and Semiconductors Using a Plane-Wave Basis Set. *Comput. Mater. Sci.* **1996**, *6*, 15−50.
(31) Kresse, G.; Furthmüller, J. Efficient Iterative Schemes for ab initio Total-Energy Calculations Using a Plane-Wave Basis Set. *Phys. Rev. B: Condens. Matter Mater. Phys.* **1996**, *54*, 11169.
(32) Thiele, G.; Rotter, H. W.; Schmidt, K. D. Crystal Structures and Phase Transformations of $RbGeBr_3$. *Z. Anorg. Allg. Chem.* **1988**, *559*, 7−16.
(33) Thiele, G.; Rotter, H. W.; Schmidt, K. D. Crystal Structures and Phase Transitions of the Tetramorhpic $RbGeI_3$. *Z. Anorg. Allg. Chem.* **1989**, *571*, 60−68.
(34) Thiele, G.; Serr, B. R. Crystal Structure of Rubidium Triiodostannate(II), $RbSnI_3$. *Z. Kristallogr. - Cryst. Mater.* **1995**, *210*, 64.
(35) Trots, D. M.; Myagkota, S. V. High-Temperature Structural Evolution of Caesium and Rubidium Triiodoplumbates. *J. Phys. Chem. Solids* **2008**, *69*, 2520−2526.
(36) Thiele, G.; Rotter, H. W.; Schmidt, K. D. Crystal Structures and Phase Transformations of Cesium Trihalogenogermanates $CsGeX_3$ (X = Cl, Br, I). *Z. Anorg. Allg. Chem.* **1987**, *545*, 148−156.
(37) Yashima, M.; Ali, R. Structural Phase Transition and Octahedral Tilting in the Calcium Titanate Perovskite $CaTiO_3$. *Solid State Ionics* **2009**, *180*, 120−126.
(38) Guennou, M.; Bouvier, P.; Kreisel, J.; Machon, D. Pressure-Temperature Phase Diagram of $SrTiO_3$ up to 53 GPa. *Phys. Rev. B: Condens. Matter Mater. Phys.* **2010**, *81*, 054115−863.
(39) Shirane, G.; Yamada, Y. Lattice-Dynamical Study of the 100 K Phase Transition in $SrTiO_3$. *Phys. Rev.* **1969**, *177*, 858−863.
(40) Tsuda, K.; Tanaka, M. Refinement of Crystal Structure Parameters using Convergent-Beam Electron Diffraction: the Low-Temperature Phase of $SrTiO_3$. *Acta Crystallogr., Sect. A: Found. Crystallogr.* **1995**, *51*, 7−19.
(41) García-Fernández, P.; Ghosh, S.; English, N. J.; Aramburu, J. A. Benchmark Study for the Application of Density Functional Theory to the Prediction of Octahedral Tilting in Perovskites. *Phys. Rev. B: Condens. Matter Mater. Phys.* **2012**, *86*, 144107.
(42) Kulkarni, S. A.; Baikie, T.; Boix, P. P.; Yantara, N.; Mathews, N.; Mhaisalkar, S. Band-gap Tuning of Lead Halide Perovskites Using a Sequential Deposition Process. *J. Mater. Chem. A* **2014**, *2*, 9221−9225.
(43) Woodward, P. M. Octahedral Tilting in Perovskites. I. Geometrical Considerations. *Acta Crystallogr., Sect. B: Struct. Sci.* **1997**, *53*, 32−43.
(44) Woodward, P. M. Octahedral Tilting in Perovskites. II. Structure Stabilizing Forces. *Acta Crystallogr., Sect. B: Struct. Sci.* **1997**, *53*, 44−66.
(45) Lufaso, M. W.; Woodward, P. M. Jahn−Teller Distortions, Cation Ordering and Octahedral Tilting in Perovskites. *Acta Crystallogr., Sect. B: Struct. Sci.* **2004**, *60*, 10−20.
(46) Howard, C. J.; Stokes, H. T. Structures and Phase Transitions in Perovskites - A Group-Theoretical Approach. *Acta Crystallogr., Sect. A: Found. Crystallogr.* **2005**, *61*, 93−111.
(47) Goldschmidt, V. M. Die Gesetze der Krystallochemie. *Naturwissenschaften* **1926**, *14*, 477−485.

DOI: 10.1021/acs.jpclett.6b00094
J. Phys. Chem. Lett. 2016, 7, 918−922